Simultaneous electrical and optical monitoring of spoke rotation, merging and splitting in HiPIMS plasma

P. Klein[1], F. Lockwood Estrin[2], J. Hnilica[1], P. Vašina[1], J. W. Bradley[2]

[1] Department of Physical Electronics, Masaryk University, Kotlářská 2, CZ-61137, Brno, Czech Republic

[2] Department of Electrical Engineering and Electronics, University of Liverpool, Brownlow Hill, Liverpool L69 3GJ, United Kingdom

E-mail: pklein@mail.muni.cz, j.w.bradley@liverpool.ac.uk

Abstract.

To gain more information on the temporal and spatial behaviour of self-organized spoke structures in HiPIMS plasmas, a correlation between the broadband optical image of an individual spoke (200 ns time-resolution) and the current it delivers to the target has been made for a range of magnetron operating conditions.

As a spoke passes over a set of embedded probes in the niobium cathode target, a distinct modulation in the local current density is observed, (typically up to twice the average value), matching very well the radially integrated optical emission intensities (obtained remotely with an ICCD camera). The dual diagnostic system allows the merging and splitting of a set of spokes to be studied as they rotate. It is observed that in the merger of two spokes, the trailing spoke maintains its velocity while the leading spoke either decreases its velocity or increases its azimuthal length. In spoke splitting, the total charge collected by an embedded probe is conserved. The results are discussed with relation to the more extensive electrical observations of Hecimovic *et al* [1] and a simple phenomenological model is developed that relates the spoke mode number m to the spoke dimensions, spoke velocity and gas atom velocity.

PACS numbers: 52.70.Kz, 52.70.Ds

Submitted to: *J. Phys. D: Appl. Phys.*

1. Introduction

High power impulse magnetron sputtering (HiPIMS) [2] is a relatively new pulsed physical vapour deposition (PVD) technique that offers some advantages over existing methods, including, very high concentrations of metal ions in the deposition flux [3], well defined ion energies during film growth [4] and the possibility of gasless operation [5]. The development of HiPIMS has seen the bringing together of conventional magnetron

sputtering [6], (i.e. in source design and magnetic topology), and state-of-the art solid state pulse power delivery technologies [7].

In common with many other low-pressure plasmas that utilize crossed electric and magnetic fields, HiPIMS discharges demonstrate plasma self-organization, in which rotating ionization zones (often called spokes) can be seen to rotate in the $\mathbf{E}\times\mathbf{B}$ direction [8, 9, 10]. This phenomenon has been observed for instance in DC magnetron sputtering (DCMS) devices [11, 12, 13], Hall thruster plasmas [14, 15, 16] and in homopolar plasma systems [17, 18]. It has also been predicted in advanced particle-in-cell Monte Carlo collision (PIC-MCC) modelling [19, 20].

Spokes in HiPIMS are believed to be regions of higher local plasma density exhibiting anomalously high positive space potentials which sit just above cathode target sheath and rotate around the closed azimuthal path of the magnetron, chiefly in the $\mathbf{E}\times\mathbf{B}$ direction. Spokes themselves are likened to double layer regions [21] (or perhaps more accurately triple layer regions [21, 22]) in which internal azimuthal electric fields, created through charge separation, cross with vacuum B-field to produce strong axial electron drifts, counter streaming ions and electrons and the associated two stream instabilities [19, 23]. This mechanism may also explain the existence of electron flares that are observed to stream away from the spoke up into the bulk plasma region [24].

A robust theory which describes how spokes form from essentially homogeneous plasma conditions is still under development. However, semi-analytical descriptions of the spatial and temporal characteristics of non-evolving spokes have been proposed. In many cases it has been observed that spokes rotate with velocities strongly correlated to the critical ionization velocity (CIV) [25] typically a few 10's kms^{-1}. However, this is not universally observed, with for instance, strong discrepancies between the CIV and spoke velocities seen in ref [13]. In low power DC and low power pulsed conditions spokes can rotate at much slower speeds, below $1\,\mathrm{kms}^{-1}$ and in a direction counter to the $\mathbf{E}\times\mathbf{B}$ drift [13, 26].

Models for spoke sustainment proposed by Anders et al [9, 27], which examine the necessity for spokes to move to regions of high ionization probability, based on the ideas contained in the CIV assumption, have provided a unified model [28] for pre-existing spokes. Phenomenological models based on fluid descriptions [23] have also aided the understanding of spoke structure and kinetic PIC-MCC simulations of similar $\mathbf{E}\times\mathbf{B}$ arrangements have clearly shown the necessity for an ionisation (the spoke) to move to positions of higher potential [19] to allow sustainment.

The formation and properties of spokes have already been identified and to some extent characterized in HiPIMS plasma using a range of non-perturbing and perturbing diagnostics tools. The former non-perturbing methods include 2-D nanoseconds broad band optical imaging [9, 29, 30], wavelength filtered imaging [29], spatial and temporally correlated optical emission spectroscopy [31] and isolated embedded target electrical (strip) probes [32]. The latter more perturbing methods have consisted mainly of single electrical probing [1, 33], the use of multi-probe arrays [1, 13, 34] and electron emitting probes [35] to detect either changes in the collected electron and ion fluxes or

modulations in the space potential. In most cases, these electrical measurements have been made in regions away from where spokes are detected optically.

The existence of spokes may have a significant influence on the deposition characteristics of HiPIMS discharges. For instance, energetic ions (background Ar and post-ionized metals) observed travelling in the axial [36, 37] and radial [38, 39, 37] directions have been correlated with the existence of the high positive space potentials [22] of rapidly rotating spokes, where such ions can be created. These fast ions, detected using retarding field analyzers [40] and sophisticated energy-resolved mass spectrometry [38, 41, 37], can bombard the substrate with considerable energy.

In HiPIMS discharge the velocity of the spokes above the target depends on the target material and running gas [25]. In high power conditions and with typical spoke speeds between 4 and 15 kms^{-1}, rotation frequencies can be from 10's to 100's kHz [9, 10, 32, 42, 43] dimensions. Discharge operating parameters such as target current density (power) and working pressure can have a large effect on the nature of the spokes. Recently, Poolcharuansin *et al* [32] and Breilmann *et al* [44] have independently shown three distinct operating regimes in HiPIMS where the spokes can be characterized as either chaotic, coherent or non-existent (indistinguishable from the background). In the stable spoke regime, spokes can be either triangular in shape or somewhat diffusive [45]. The mode number m, was found to depend largely on the discharge current [8]. At low discharge currents single spokes are observed which evolve into multiple spokes ($m > 1$) as the magnetron power ramps up during the pulse, however above a certain threshold the system reverts to a single mode again [1, 43]. Here spokes may become uniformly distributed around the whole racetrack region of the target so revealing an azimuthally symmetric plasma emission [43, 46]. Chaotic spokes can have a variety of shapes, but are short-lived, irregularly spaced with no easily discernible mode number.

Recently, the interesting phenomena of spoke splitting and merging was observed by Hecimovic *et al* [1] using an array of phase correlated azimuthally arranged Langmuir probes around the discharge perimeters. A mechanism for this was proposed by the authors based on the speeding up or slowing down of individual spokes as they rotate. Here, a fast 2-D optical imaging of rotating spokes is combined with simultaneous target measurements of local current density as they pass over a particular region of the target. This allows us to relate the shape of spokes seen optically to their "electrical" footprint on the target and to observe the merging of spokes by the both techniques and compare and contrast the results to those in [1].

2. Experimental set-up

The experimental study was performed using an Alcatel SCM 650 magnetron sputtering system, housing a 75 mm diameter circular magnetron (Kurt J. Lesker) fitted with a niobium target of 99.95% purity (Testbourne Ltd). The total magnetic field strength 1 mm above racetrack was measured to be 72 mT using a Hall probe MI 2010T (Magnetic Instrumentation Inc.). The deposition chamber was pumped by a turbo-molecular

pump backed by a roots pump to a base pressure below 1×10^{-4} Pa. The pressure was measured using both a Capacitance Baratron MKS gauge and a PKR 251 compact full vacuum range gauge (Pfeiffer Ltd). Argon gas with 99.999% purity was supplied to the vessel at flow rate in a range of 1 – 140 sccm (standard cubic centimetre per minute) to provide working pressures from of 0.14 – 5 Pa. A metal substrate holder was positioned 4.5 cm from the target although no coatings were made here.

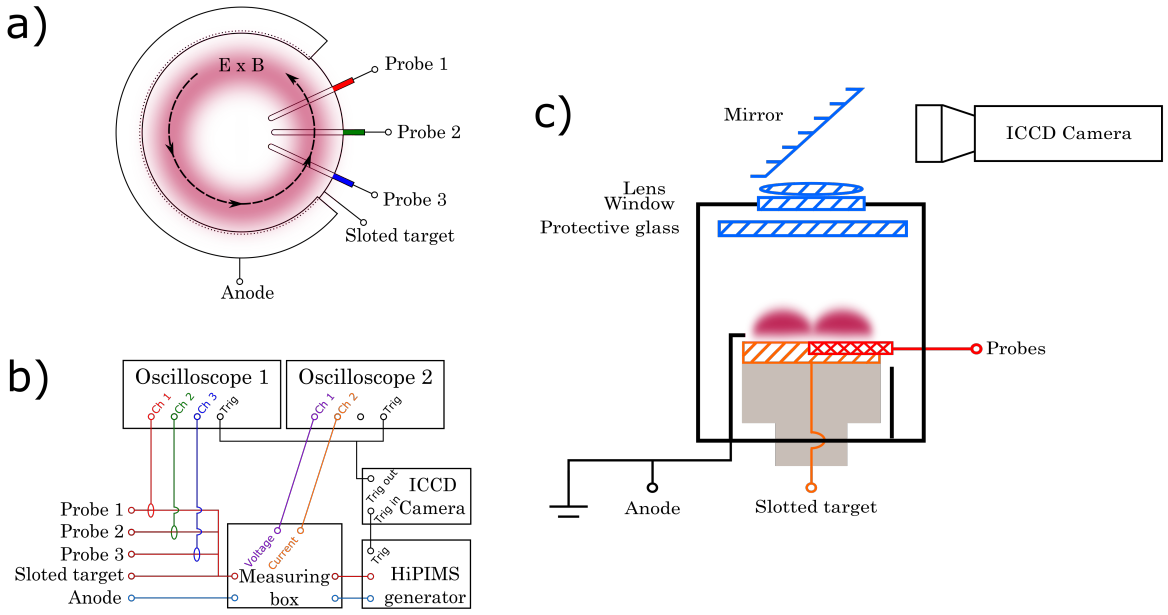

Figure 1. Schematic drawing of a) the top view of the target strip probe experimental setup and b) the strip probe electrical arrangement and the optical imaging arrangement.

The discharge was driven by a dual-channel Melec SIPP 2000 HiPIMS generator, capable of providing peak discharge currents up to 500 A and voltages up to -1000 V. Here, we chose a pulse length (on-time) of 200 μs with a repetition rate of 5 Hz. The output cables from the generator were looped nine times through a ferrite ring to suppress fast high-amplitude oscillation that could damage the pulser. In addition, to aid plasma breakdown an Auxiliary Dressler Cesar 500 radio frequency (13.56 MHz) generator with mean power of 20 W connected to the substrate holder was used as a pre-ionizer. RF matching was adjusted to maintain the reflected power below 2 W.

To determine the local target current density associated with individual spokes the target was segmented, incorporating three 2 mm wide flush-mounted rectangular niobium strips (same purity as the target) to act as isolated probes. We denote the strips with number 1, 2 and 3 and colours red, green and blue for clarity of presentation in the results section below. The strip probes were placed in machined slots at three angular positions (25° from each other) around the target in manner similarly to that shown in [32]. To accommodate the strip probes, the outer anode shield of the magnetron was cut away as shown in Fig. 1a, which unavoidably marginally influenced the discharge

in the vicinity of the strip probes, as seen by a 15% drop in the intensity of the optical emission signal compared to the rest of the target.

The three individual strip probes were connected directly to the HiPIMS power supply as shown in Fig. 1b, allowing each to maintain a potential equal to that of the rest of the target. Their contributions to the total discharge current were measured separately using three Pearson current probes (Model 2877 with 1 V/A). All three probe signals were recorded using the single shot mode facility of a LeCroy WaveRunner 6100A digital oscilloscope with a 4 ns sampling interval. The waveforms for the total discharge voltage and discharge current were measured using a measuring system integrated in the Melec generator, in which cathode voltages and currents in the range 0 – 1000 V and 0 – 500 A respectively were displayed as voltage signals in the range 0 – 10 V. These readings were recorded using a Keysight Infiniium DSO-S 204A oscilloscope working in single shot mode with 4 ns sampling interval.

The 2-D optical imaging arrangement to observe the rotating spokes is shown in Fig. 1c. The system consisted of an internal protective glass sheet, a quartz vacuum window, an external convex lens with focal length 50 mm, a 45° mirror and an intensified charge coupled device (ICCD) camera. The protective glass was placed on rotatable substrate holder 4.5 cm above the target to protect the chamber window from the coating build-up and maximize the experimental runtime. The images were taken by the ICCD camera PI-MAX 3 (Princeton Instruments) equipped with Nikkor MF 80 – 200 f/4.5 camera lens. The ICCD camera worked in dual image feature mode (DIF), enabling the capture of two snapshots during one HiPIMS pulse with a 3 μs delay between them. The start of the exposure was synchronized with the discharge pulse and the ICCD detector was gated through an electronic shutter with a gate width of 100 ns. The camera captured grey-scale images with 1024×1024 pixels resolution, which were later converted to (false) colour using MATLAB Jet(72) software.

3. Results and discussion

3.1. Comparison of electrical and optical characteristics of spokes

In a previous study, using flush mounted target strip probes, periodic oscillations in the local current density detected by the strips were attributed to the presence of rotating spokes [32]. Phase information between azimuthally separated probes provided data on the spoke mode number and the rotation velocity. However, visual confirmation of spokes was not possible in that arrangement. Here through the simultaneous use of strip probes and fast optical imaging we able to confirm that strip probe current modulations are in fact due to spokes and also have the means to compare their electrical and optical characteristics.

Initially, we chose to operate the magnetron at a single pressure and observe the evolution of spokes through the HiPIMS pulse. Fig. 2 shows the discharge current waveform for a pulse at a pressure of 5 Pa and pulse average power of 73 W. It should

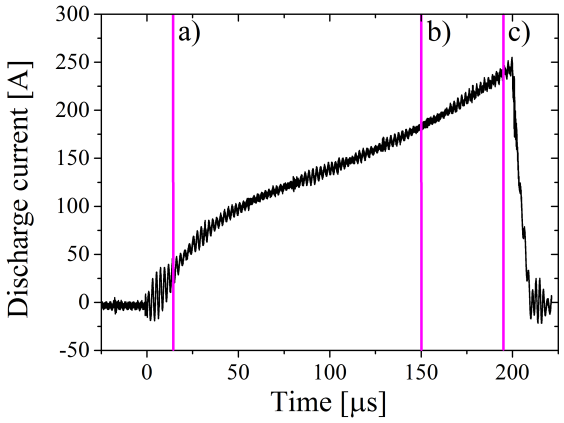

Figure 2. A typical discharge current waveform for a pressure of 5 Pa, cathode voltage 571 V and average power of 73 W. The violet vertical lines indicate times when the images shown in following Fig. 3 are taken.

be noted that small amplitude oscillations in the cathode voltage and discharge current with the frequency of 1 MHz are present in the waveform, as reported earlier by Maszl *et al* [22].

Fig. 3 shows three representative images of the broadband plasma emission and the corresponding strip probe current signal for three different instantaneous discharge current readings (30, 180 and 240 A, see violet vertical lines in Fig. 2) during a pulse of time-average power 73 W at a pressure of 5 Pa. The emission intensities are normalised to a maximum intensity within given image. As see in Fig. 3a, early in the pulse at very low discharge currents, spokes are not yet fully developed and the plasma emission is homogeneous with no periodic structures in the strip probe signal, only a gradual increase in the current as the total discharge current builds up. Progressing through the pulse as the discharge current grows - see Fig. 3, and spokes are formed. At a total measured discharge current of 185 A six well differentiated diffusive spokes are clearly visible in Fig. 3b with their harmonic signature signal on the strip probe. At 240 A the spokes becomes triangular in shape, see Fig. 3c, as observed in many optical studies (e.g. see [8, 9, 42, 43]), this is easily discernable in the strip probe current signal as the spoke passes with a shallow rise in current followed by a more rapid fall.

Both the diffusive and triangular spokes are observed at a pressure of 5 Pa. Decreasing of the pressure leads to a decrease in spoke mode number for the same discharge current. Additionally, only the triangular spoke shape with very precisely defined trailing edge of the spokes is observed. The well-defined spoke shape at low pressure enables to unambiguously determine the position of individual spoke on camera images. Using the unique dual image feature of the PI-MAX 3, two consecutive plasma emission images were taken at an operating pressure of 0.14 Pa and a pulse-average power of 48 W. These are shown in Fig. 4a-b at a time corresponding to a discharge current of 210 A.

In both images the position of each strip probe is indicated by a different colour as

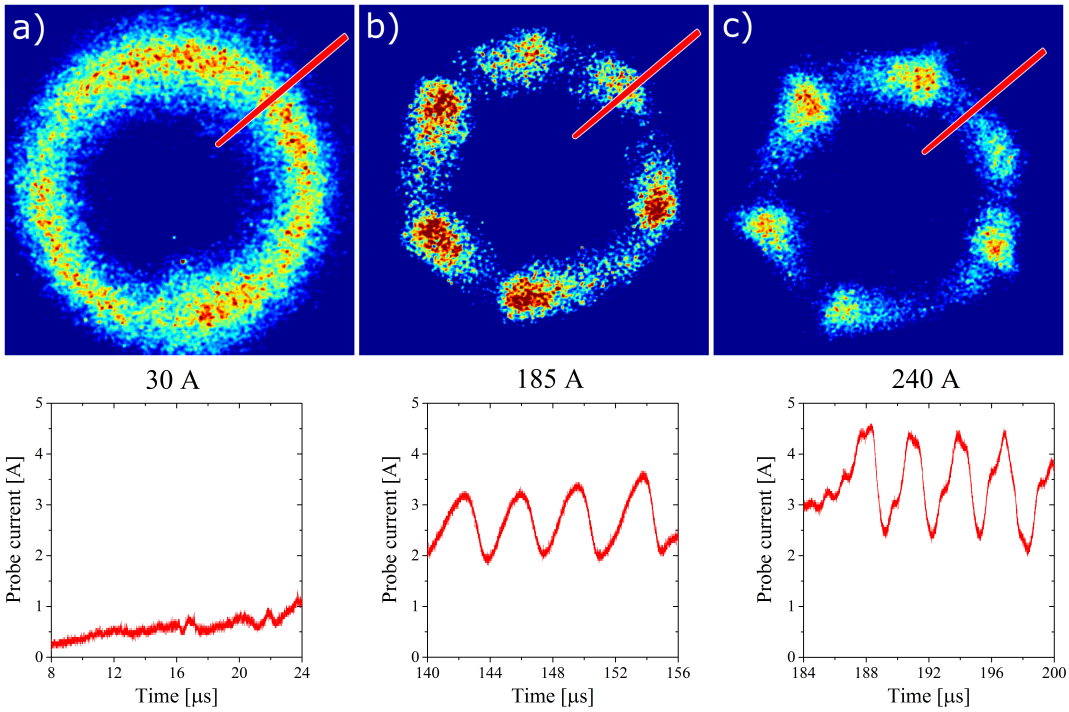

Figure 3. Broadband emission images of the full target with and corresponding strip probe current measurements (strip 1) for an operating pressure of 5 Pa, cathode voltage of 571 V and discharge currents of a) 30 A b) 185 A c) 240 A as is indicated by violet vertical lines in Fig. 2. Note: intensities are normalized to maximum intensity at the given picture.

described in section 2. Three well developed triangular spokes ($m = 3$) are identified rotating in a counter-clockwise direction with a velocity of 13.4 kms^{-1} (calculated using a racetrack length of 157 cm, a 3 μs time delay between images and a 92 degrees angular shift between spoke trailing edges from Fig. 4a-b). The corresponding current signals for the three strip probes are shown in Fig. 4c. The two violet vertical lines (at time of 191 μs and 194 μs) indicate when the 2-D images were taken in Fig. 4a and b. From the current traces a spoke rotation velocity of 13.5 kms^{-1} (the gradient of the cyan line in Fig. 4c) and rotation period of 11.6 μs are determined, values extremely close to that determined optically.

To make a direct comparison between the broadband optical emission intensities and the strip probe time traces of current delivered to the target from spoke structures, the 2-D optical data has been transformed to 1-D by integrating over the radial direction. The 2-D images in Fig. 4a-b have been transformed in this manner and are shown in Fig. 5a-b together with the corresponding current waveform (from strip 1 shown in red). The time-trace of the transformed optical data matches well the strip probe current traces, i.e. the length of the spokes are equal, the phases are consistent and maxima and minima appear at the same time.

In a simplistic view, if we do not consider the secondary electron current from the target, the current traces seen by the target strip probe (denoted by I_s) will be

determined by the local electron density adjacent to the cathode sheath n_e and the speed of the incoming ions (given by the local electron temperature T_e through the Bohm criteria with $I_s \sim n_e T_e^{1/2}$). Since the form of the time traces of the intensity of the broadband optical signal matches well the electrical measurements of ion current delivered to the target, it suggests the optical signal must have a dependency on n_e and T_e somewhat close to $n_e T_e^n$ with $n \sim 1/2$.

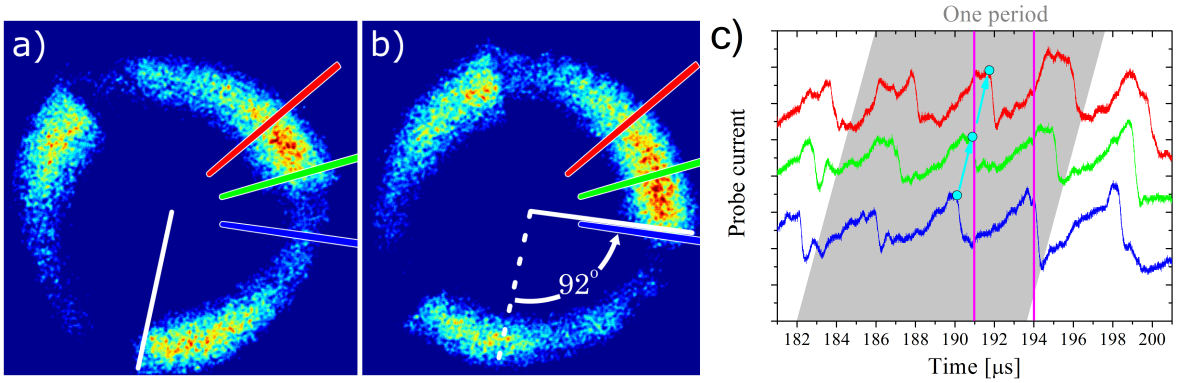

Figure 4. a) and b) two consecutive 2-D emission images of the whole target from a single pulse and c) the corresponding strip probe waveforms (red, green and blue) for an operating pressure of 0.14 Pa, instantaneous discharge current of 210 A and cathode voltage of 628 V. The vertical violet lines at time of 191 μs and 194 μs indicate when the optical images a) and b) were taken. The grey background depicts a spoke rotation period.

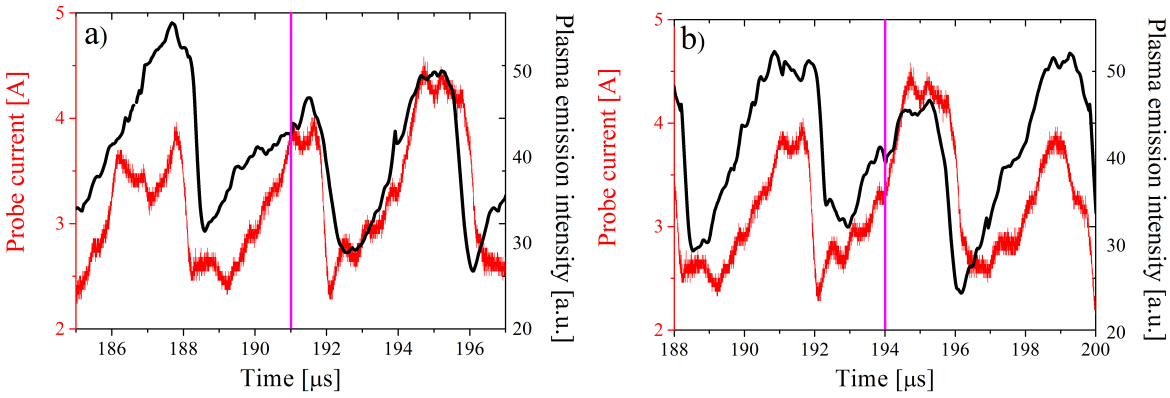

Figure 5. Transformation of 2-D optical intensities shown in Fig. 4a-b to 1-D time traces (black) together with the corresponding strip probe (probe 1 in Fig. 1a) waveform (red) for an operating pressure of 0.14 Pa and average discharge power of 48 W at an instantaneous discharge current of 210 A and cathode voltage of 628 V. The vertical violet lines at time of 191 μs (graph a) and 194 μs (graph b) indicate times when the original images in Fig. 4a-b were taken.

3.2. Observations of spokes merging

The dual diagnostic arrangement allows a detailed study of the time evolution of spokes as they rotate, including the merging and splitting of spokes.

In terms of merging, the present hypothesis proposed by Hecimovic *et al* [1] states that consecutive spokes merge as the discharge current grows and spokes duly enlarge. This process results in increased local sputtering of the target and higher buffer gas rarefaction. The lack of buffer gas atoms slows the ionization rate, consequently causing the following spoke to shrink, while providing less stopping power for electrons allowing the small spoke to catch up with the larger one to unite and form one large spoke.

The merging of spokes in our system can clearly be seen through the simultaneous use of optical imaging and strip probe monitoring as shown in Fig. 6a-c for an operating pressure of 0.14 Pa, pulse average power of 48 W and instantaneous discharge current of 210 A. From the high-speed camera images we can define the merging process to have taken place when two separated spokes, each with distinct trailing edges, coalesce to form one spoke with single trailing edge. In Fig. 6a, the initial mode number is $m = 3$, with spokes identified as numbers 1, 2 and 3. Some 3 μs later spokes 2 and 3 have clearly merged, however retaining a maximum plasma emission intensity close to that of the separate spokes before the merging process (see Fig. 6a). In the merged spoke (Fig. 6b) the plasma emission intensity is redistributed and its maximum is at the trailing edge of the spoke. The same pattern can be deduced from the strip probe waveforms in Fig. 6c, with the current maxima of the leading spoke vanishing and the resulting current waveform resembling a single larger triangular shape. Spoke number 1 did not change its shape during the 3 μs delay time between the images shown in Fig. 6a-b. The angular shift between trailing edges of the spoke 1 in Fig. 6a) and Fig. 6b) is 95 degrees. The same angular shift is determined between trailing edge of spoke 3 (Fig. 6a) and trailing edge of merged spokes 2 and 3 (Fig. 6b). Therefore, it appears that spokes 1 and 3 maintained their velocities during the merging process, however from the measured data it is unclear what happened with the spoke 2. Either spoke 2 slowed down, or one or both of spokes 2 and 3 increased their azimuthal length. This somewhat questions the mechanism proposed by Hecimovic *et al* [1], where the trailing spoke catches up with leading one due to its increased velocity.

3.3. Observation of spokes splitting

In our experiments, the number of spokes increase with the increase of the discharge current during a HiPIMS pulse, which was also reported earlier [8]. There seems to be two possible scenarios for the increase in the number of spokes: 1) spontaneous spoke creation in which a new spoke appears in a gap between two neighbouring spokes, in order to provide the necessary ion current to the target; 2) a large spoke separates into parts as it rotates. The former possibility however has not yet been detected, however in this study spoke splitting is readily observed optically and electrically with a typical example shown in Fig. 7a-b for an operating pressure of 2 Pa, a pulse average power of

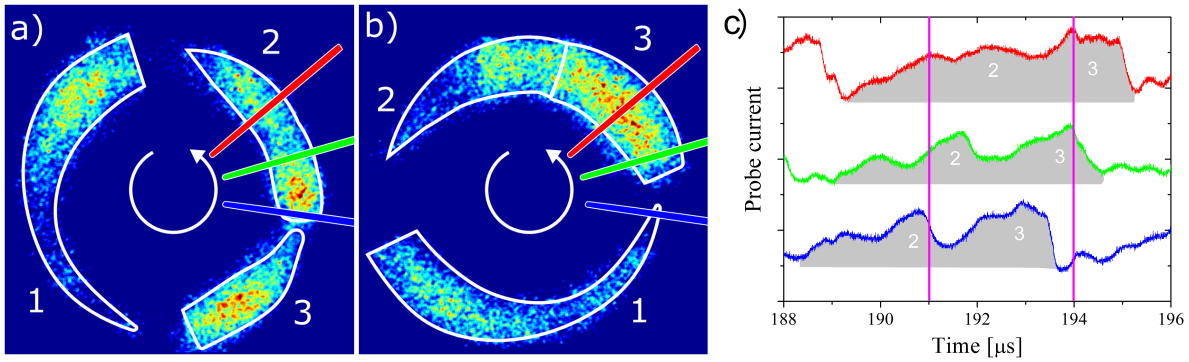

Figure 6. a) and b) two consecutive plasma emission images (3 μs apart) from one single pulse and c) the corresponding current waveforms from all three strip probes for an operating pressure of 0.14 Pa, pulse average power of 48 W, an instantaneous discharge current of 210 A and cathode voltage of 628 V. The vertical violet lines at time of 191 μs and 194 μs indicate times when the optical images a) and b) were taken.

58 W and instantaneous discharge current of 220 A.

The spoke in question has a well developed triangular shape as identified in Fig. 7a. In the time it takes to reach the red strip probe from the blue one (3 μs), the spoke has clearly split. In fact, differentiation of the structure begins at the green strip probe (1.5 μs) with identification of two maxima in the strip probe current (Fig. 7c). At this point, the leading maximum is more pronounced than the trailing one. As the spoke evolves, the first maximum intensifies further and narrows in the azimuthal direction, while the trailing peak broadens.

The total charge collected by the strip probe from the spoke in question is the integral of the current over time as it passes, depicted by the grey area under the curve in Fig. 7c. This area does not change as the spokes pass all three strip probes, indicating that the charge, and therefore the spoke density, is conserved during the splitting process.

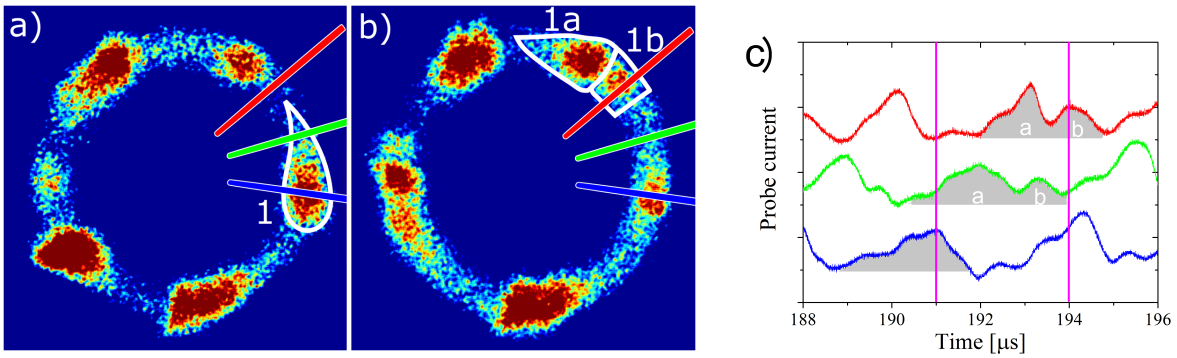

Figure 7. a) and b) two consecutive 2-D broadband emission images of the target from one single pulse and c) the corresponding current waveforms from all three strip probes for pressure of 2 Pa, pulse average power of 58 W, instantaneous discharge current of 220 A and cathode voltage of 580 V. The vertical violet lines at time of 191 μs and 194 μs indicate times when the optical images a) and b) were taken.

3.4. Spoke evolution over multiple rotation periods

Both electrical and optical emission observations in sections 3.2 and 3.3 show that the time-scales for spoke merging and splitting are typically $\sim 3\,\mu$s, which is somewhat shorter than the period of rotation ($\sim 12\,\mu$s). Since the area covered by the strip probes is only about 14% of the total target area, we only record a part of the spoke merging and splitting events. The merging and splitting processes generate a new configuration where the spoke mode number changes. A further analysis (below) in which we record data over several consecutive rotational periods has revealed that these configurations are only quasi-stable in time.

Observing spokes over longer period has the problem that the plasma parameters change as the HiPIMS discharge current increases. Here we choose to monitor spokes at our lowest pressure of operation (0.14 Pa) as the corresponding low spoke number enables us to determine the spoke rotational period precisely and moreover the spoke mode number is rather independent of the discharge current. Fig. 8 shows the evolution of the three strip probe currents (blue, green and red) over three rotational periods (denoted as 1st, 2nd and 3rd), each period with a duration of $12\,\mu$s. We should note that the third period in Fig. 8 is identical to that shown in Fig. 6. From the phase relationships of the measured strip probe currents (from all three strips) obtained prior to $188\,\mu$s, the spoke velocities before their merger at $194\,\mu$s have been calculated. It was observed that the spoke speeds did not vary more than 2.5% about $13.3\,\mathrm{kms}^{-1}$, $24\,\mu$s preceding the merger.

Inspection of Fig. 8 shows for instance in the 3rd period, that two small spokes (denoted as 1a and 1b), merge into one larger spoke (denoted as 1): a phenomena confirmed by fast camera observations in Sec. 3.2. This situation can also be seen in the earlier 2nd period, where all three probes detect a large spoke 2 and two half-sized spoke 1a and 1b. We therefore argued that no merging or splitting events have occurred outside the scanned area between the 2nd and 3rd periods.

In the early part of 1st period again three spokes were detected (at the blue and green probes) however in this case spoke 1 was large and spokes 2a and 2b were half-sized. These two smaller spokes 2a and 2b then merge as they pass over the strip probe scanning area forming two large spokes 1 and 2 by the time they reach the red strip probe. In fact, inspection of Fig 8 reveals that over the three recorded periods the spoke mode number m is constantly changing, with $m = 3$ (spokes 1, 2a and 2b) transforming to $m = 2$ (spokes 1 and 2), then to $m = 3$ (spokes 1a, 1b and 2) and finally back to $m = 2$ (1 and 2).

Therefore, in our chosen operating conditions at least, the merging and splitting processes do not lead to a new stable spoke configuration but the system seems to oscillate between the $m = 2$ and $m = 3$ modes. This quasi-stationary, non-symmetrical behaviour of spokes may indicate that the condition necessary to actually sustain two or three large stable spokes is not met. In the next section, we develop a simple model that can predict conditions for a stable spoke mode configuration.

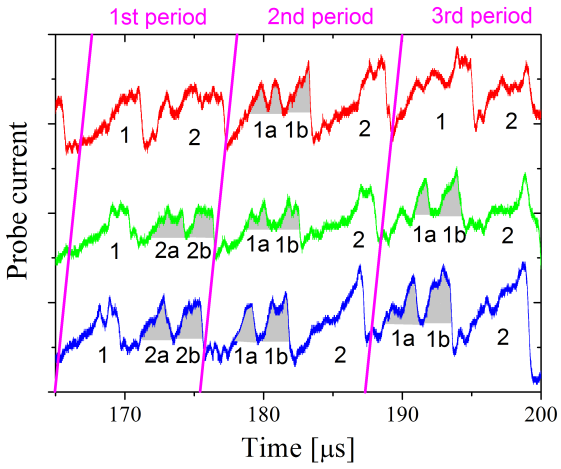

Figure 8. Current waveforms from all three strip probes over three rotation periods for an operating pressure of 0.14 Pa, a pulse average power of 48 W, an instantaneous discharge current of 210 A and cathode voltage of 628 V. The different spokes are identified as 1 and 2. Spoke 1 in the 3rd period was used to describe the merging process in Fig. 6).

4. Phenomenological model of spoke organisation

In preceding section, observations of spoke merging and splitting were described. From the multiple measurements at given experimental conditions (pressure, discharge current etc.) only slight variation from average mode number m was observed (typically a change of $\triangle m = 1$). The spokes are merging and splitting over time, but the average mode number m is easy to define.

The aim of this section is to present a model predicting a stable mode number m. The model presumes that the presence of Ar in the spoke is essential for spoke sustainment. The contribution of the sputtered Nb atoms in spoke sustainment is neglected as the Nb ion impinging the target do not provide sufficient secondary electrons. The flux of sputtered Nb from the target, however, displaces Ar from the spoke and prohibits its return to the target vicinity. Ar rarefaction will then force the spoke to move to an advancing location. If in time of the spoke arrival Ar refilled the space left by the forgoing spoke, there is no driving force for spokes to merge. However at insufficient Ar presence, the spoke diminishes in size, or merges with neighbouring spoke. On the other hand at the excessive presence of Ar, the spoke to grows. The spoke may grow to the point where it is more energy efficient for the system to increase the spoke mode number. The spoke then splits into two smaller spokes.

Consider the whole racetrack circumference R being symmetrically covered by m identical spokes each with length l, width w and height h rotating with velocity v_{sp} as depicted in Fig. 9. The transition time τ_{tr} between neighbouring spokes (to move from

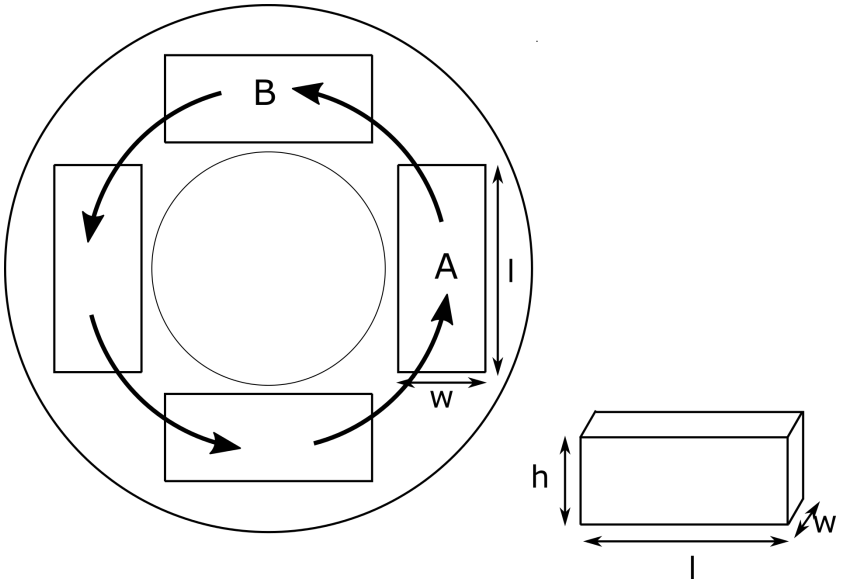

Figure 9. Schematic diagram of the proposed spoke model.

point A to point B) is given by:

$$\tau_{\mathrm{tr}} = \frac{R}{m\, v_{\mathrm{sp}}}. \tag{1}$$

The fast sputtered Nb particles originating from the forgoing spoke move perpendicularly to the target surface evacuating the area of the point B. The evacuation process time τ_{sp} is given by:

$$\tau_{\mathrm{sp}} = h \sqrt{\frac{M_{\mathrm{t}}}{2\, e\, E_{\mathrm{B}}}} \tag{2}$$

where M_{t} is atomic mass of target atoms (i.e. Nb) and E_{B} is their surface binding energy. Ar refilling takes place at point B with the refill time τ_{rf} given by:

$$\tau_{\mathrm{rf}} = \frac{L}{v_{\mathrm{Ar}}} \tag{3}$$

where v_{Ar} is the Ar velocity and L is the characteristic length for Ar refilling. The refilling is possible from both sides and from the top of the spoke, thus L is a smaller value from either $w/2$ or h.

During the Nb evacuation at point B, Ar refilling is strongly obstructed. Assuming that during evacuation of the sputtered Nb at the point B, argon gas can not return at all, the foregoing spoke arriving to the point B will find a sufficient amount of Ar gas for spoke sustainment when

$$\tau_{\mathrm{tr}} = \tau_{\mathrm{sp}} + \tau_{\mathrm{rf}}. \tag{4}$$

In equation (4), if conditions in the plasma persist such that $\tau_{\mathrm{tr}} < \tau_{\mathrm{sp}} + \tau_{\mathrm{rf}}$ and considering v_{sp} to be constant then the system will rapidly evolve so that m decreases, i.e. through spoke merging. If $\tau_{\mathrm{tr}} > \tau_{\mathrm{sp}} + \tau_{\mathrm{rf}}$ a spoke will moves into a region that can sustain it and m is free to remain at its current value or increase through spoke splitting.

Substituting equations (1), (2) and (3) into equation (4) we get:

$$\frac{R}{m\,v_{\rm sp}} = h\sqrt{\frac{M_{\rm t}}{2\,e\,E_{\rm B}}} + \frac{L}{v_{\rm Ar}} \tag{5}$$

We can now compare the model to our observations, and choose to do this at conditions in Sec. 3 with a pressure of 0.14 Pa. However use of equation 5 requires knowledge of the spoke dimensions. In the model the spoke is represented by a block, however in reality triangular spokes were observed. Therefore, the width w of the spoke may be derived from the 2-D images, either as a maximum value obtained at the trailing edge of the spoke parallel to magnetic field ($w = 1\,$cm), or its average value ($w = 0.5\,$cm). The height h of the spoke was not measured, however it is assumed to be approximately the half of the spoke width, which is consistent with side-on images obtained by Anders *et al* [9]. The observed spoke rotation velocity $v_{\rm sp}$ is determined by complex physical process of the plasma, yet to be fully understood. It can be calculated for instance from the CIV model [25] or from the model proposed by Anders [27]. However, here our measured spoke rotation velocity of $13.4\,{\rm kms}^{-1}$ exceeds predictions based on both these models, and therefore we chose to use our experimentally determined value of $v_{\rm sp}$ in equation (5) rather than determine it from other parameters. Consequently, substituting our spoke dimensions, the measured spoke rotation velocity, table values for $U_{\rm B} = 5.9\,$eV [47], $M_{\rm t}({\rm Nb}) = 92 \times 1.66 \times 10^{-27}\,$kg and a mean racetrack circumference $R = 14\,$cm, the equilibrium mode number as a function of Ar atom velocity $v_{\rm Ar}$ is obtained, see Fig. 10. Here we calculate m for a number of realistic spoke dimensions and in include in the figure the equivalent Ar gas temperature $T_{\rm g}$ through

$$T_{\rm g} = \frac{\pi M_{\rm Ar} v_{\rm Ar}^2}{8k_{\rm B}}, \tag{6}$$

where $M_{\rm Ar}$ is Ar atomic mass and $k_{\rm B}$ is Boltzmann's constant.

A pressure of 0.14 Pa an average mode number 3 was measured. For the three spoke dimensions chosen, the calculated Ar atoms velocities required to sustain $m = 3$ spokes are $0.9\,{\rm kms}^{-1}$, $1.2\,{\rm kms}^{-1}$, or $2.5\,{\rm kms}^{-1}$ respectively (see Fig. 10). The equivalent gas temperature are 1500 K, 2700 K and 11800 K. A higher temperature is required for larger spoke dimensions. Although these temperatures appear high, Vitelaru *et al* [48] measured argon temperatures of up to 1400 K, with the temperature correlated to the peak discharge current. Temperature of the order of 1000 K and low mode numbers (e.g. $m = 3$) are consistent with small spokes in this model.

Assuming that Ar atoms follow a Maxwell-Boltzmann velocity distribution with a temperature of 1000 K and with spoke dimensions of $w = h = 0.5\,$cm (blue line in Fig. 10), the fraction of Ar atoms from an essentially infinite external reservoir contributing to refilling and thus sustaining of the spokes was evaluated to be 6% of total distribution.

So to sustain a spoke moving into a region exited by a proceeding spoke, it is not necessary for Ar to return back completely. A certain critical amount of Ar gas is required to ensure a stable configuration in m spokes. At higher argon pressures more

spokes can be sustained simultaneously because of the larger reservoir of Ar, containing more particles, that can participate in building up to a critical amount required in the target vicinity.

We should note that key parameters such as discharge current and pressure, known to influence the spoke mode number, are not explicitly included in equation 5. However, the input variables v_{Ar}, L (the minimum of $w/2$ or h) and h will all be determined directly or indirectly on the process parameters.

Fig. 10) shows that the spoke width w has a strong influence on the outcome of the model. For instance, the mode number can reduce by about $\triangle m = 1$ for an increase in w from 0.5 to 1 cm. However, such a change in the spoke width is not observed experimentally here, and therefore one could argue according to the model that the local argon gas velocity v_{Ar} (determined by the gas temperature) is the key parameter influencing the mode number.

In future studies, the model could be validated somewhat by measuring the Ar gas temperature T_{g} through optical diagnostics [48] as a function of operating parameters (i.e. discharge current and pressure) with the observed mode numbers compared to the model predictions, using v_{Ar} as an input parameter (determined from the T_{g} measurements).

Overall, the model provides realistic estimates of the spoke mode number that can sustained for particular spoke and plasma conditions, and a framework for further development of more sophisticated modelling for the prediction of m.

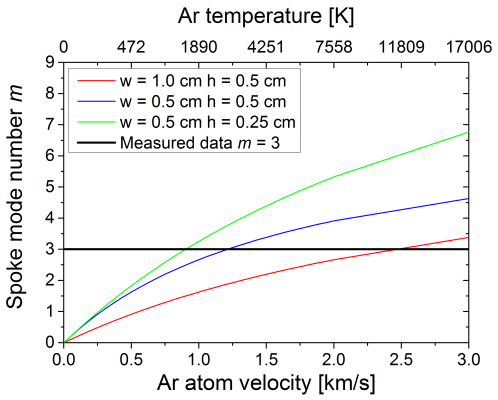

Figure 10. The predicted spoke mode number m as a function of Ar atom velocity (and equivalent temperature) for different spoke dimensions.

5. Conclusions

Using simultaneous fast 2-D optical imaging and local discharge current measurements on the target, the signature of coherent spokes rotating above the racetrack in a HiPIMS discharge have been determined. The two techniques, namely, 200 ns time-resolved remote ICCD imaging and the incorporation of embedded and isolated strip probes in

the target show the same profiles of passing spoke structures, with a sharp trailing edge, consistent with optical measurements in the literature. The target strip probes show a distinct modulation in the local current density, typically up to twice the average value associated with the spoke, as it delivers more current that the background plasma between spokes.

The system allows the merging and splitting of spokes to be clearly identified. At certain times two spokes with similar sizes and intensities merged into one larger spoke. During the merging process the trailing spoke retained its velocity, however it is unclear whether the leading spoke decreased its velocity or the merging spokes increased their azimuthal lengths. In the merged spoke both the plasma emission intensity and current collected by the embedded probes is redistributed to have their maximum at a trailing edge. The results are discussed with relation to the more extensive electrical observations of Hecimovic *et al* [1]. The reverse process, in which spokes split was also observed. The total charge collected by the strip probe during the spoke splitting was conserved. After spoke merging or splitting events, the new spoke configuration was not always stable in time. Often the large spoke would split into two smaller spokes only to reform a short time later.

The development of a simple phenomenological model has allowed us to relate the stable configuration of m spokes to their dimensions, rotation velocity and the velocity of the background Ar gas atoms. To sustain a stable spoke configuration, a sufficient time is required, between spokes as they pass a point, so that Ar can refill the space left by leading spoke. At a particular set of operating conditions (pressure of 0.14 Pa and time-average power of 48 W) and using spoke dimensions of width and height of 0.5 cm, our average observed mode number of $m = 3$ would require refilling by the Ar atoms with velocity at least 1.2 kms^{-1}. Thus only the fast Ar atoms which arrived in time to the area left by the leading spoke contribute to the sustainment of the following spoke.

Acknowledgements

This research has been partially financially supported by the Czech Science Foundation in frame of the project 15-00863S by the project CZ.1.05/2.1.00/03.0086 funded by European Regional Development Fund and the project LO1411 (NPU I) funded by Ministry of Education Youth and Sports of Czech Republic. F. L. Estrin would like to thanks EPSRC for their studentship funding under the Fusion Doctoral Training Network, grant number EP/H012605/1.

References

[1] Hecimovic A, Schulz-von der Gathen V, Böke M, von Keudell A and Winter J 2015 *Plasma Sources Sci. Technol.* **24** 045005

[2] Sarakinos K, Alami J and Konstantinidis S 2010 *Surf. Coat. Technol.* **204** 1661–1684

[3] Bohlmark J, Lattemann M, Gudmundsson, J T, Ehiasarian A P, Gonzalvo Y A, Brenning N and Helmersson U 2015 *Thin Solid Films* **515** 1522–1526

[4] Alami J, Eklund P, Andersson J M, Lattemann M, Wallin E, Bohlmark J, Persson P and Helmersson U 2007 *Thin Solid Films* **515** 3434–3438
[5] Andersson J and Anders A 2008 *Appl. Phys. Lett.* **92** 221503
[6] Kelly P J and Arnell R D 2000 *Vacuum* **56** 159–172
[7] Helmersson U, Lattemann M, Bohlmark J, Ehiasarian A P and Gudmundsson J T 2006 *Thin Solid Films* **513** 1–24
[8] Kozyrev A V, Sochugov N S, Oskomov K V, Zakharov A N and Odivanova A N 2011 *Plasma Phys. Rep.* **37** 621
[9] Anders A, Ni P and Rauch A 2012 *J. Appl. Phys.* **111** 053304
[10] Ehiasarian A P, Hecimovic A, De Los Arcos T, New R, Schulz-Von Der Gathen V, Böke M and Winter J 2012 *Appl. Phys. Lett.* **100** 114101
[11] Anders A, Ni P and Andersson J 2014 *IEEE Trans. Plasma Sci.* **42** 2578–2579
[12] Panjan M, Loquai S, Klemberg-Sapieha J E and Martinu L 2015 *Plasma Sources Sci. Technol.* **24** 065010
[13] Hecimovic A, Maszl C, Schulz-von der Gathen V, Böke M and von Keudell A 2016 *Plasma Sources Sci. Technol.* **25** 035001
[14] Parker J, Raitses Y and Fisch N 2010 *Appl. Phys. Lett.* **97** 091501
[15] McDonald M S and Gallimore A D 2011 *IEEE Trans. Plasma Sci.* **39** 2952–2953
[16] Ellison C L, Raitses Y and Fisch N J 2012 *Phys. Plasmas* **19** 013503
[17] Angerth B, Block L, Fahleson U and Soop K 1962 *Nucl. Fusion Suppl.* (Part 1) 39–46
[18] Himmel G and Piel A 1973 *J. Phys. D: Appl. Phys.* **6** L108–L111
[19] Boeuf J P and Chaudhury B 2013 *Phys. Rev. Lett.* **111** 155005
[20] Pflug A, Siemers M, Melzig T, Schäfer L and Bräuer G 2014 *Surf. Coat. Technol.* **260** 411–416
[21] Anders A, Panjan M, Franz R, Andersson J and Ni P 2013 *Appl. Phys. Lett.* **103** 19–23
[22] Maszl C, Breilmann W, Benedikt J and von Keudell A 2014 *J. Phys. D: Appl. Phys.* **47** 224002
[23] Gallian S, Hitchon W N G, Eremin D, Mussenbrock T and Brinkmann R P 2013 *Plasma Sources Sci. Technol.* **22** 055012
[24] Anders A 2014 *Appl. Phys. Lett.* **105** 244104
[25] Brenning N and Lundin D 2012 *Phys. Plasmas* **19** 093505
[26] Yang Y, Liu J, Liu L and Anders A 2014 *Appl. Phys. Lett.* **105** 254101
[27] Anders A 2012 *Appl. Phys. Lett.* **100** 2010–2015
[28] Brenning N, Lundin D, Minea T, Costin C and Vitelaru C 2013 *J. Phys. D: Appl. Phys.* **46** 084005
[29] Liebig B, Braithwaite N S J, Kelly P J and Bradley J W 2010 *Thin Solid Films* **519** 1699–1704
[30] Andersson J, Ni P and Anders A 2013 *Appl. Phys. Lett.* **103** 054104
[31] Britun N, Minea T, Konstantinidis S and Snyders R 2014 *J. Phys. D. Appl. Phys.* **47** 224001
[32] Poolcharuansin P, Estrin F L and Bradley J W 2015 *J. Appl. Phys.* **117** 163304
[33] Vlček J, Kudláček P, Burcalová K and Musil J 2007 *Europhys. Lett.* **77** 45002
[34] Yang Y, Zhou X, Liu J and Anders A 2016 *Appl. Phys. Lett.* **108** 034101
[35] Rauch A, Mendelsberg R J, Sanders J M and Anders A 2012 *J. Appl. Phys.* **111** 083302
[36] Lundin D, Stahl M, Kersten H and Helmersson U 2009 *J. Phys. D: Appl. Phys.* **42** 185202
[37] Franz R, Clavero C, Kolbeck J and Anders A 2016 *Plasma Sources Sci. Technol.* **25** 015022
[38] Lundin D, Larsson P, Wallin E, Lattemann M, Brenning N and Helmersson U 2008 *Plasma Sources Sci. Technol.* **17** 035021
[39] Čada M, Adámek P, Straňák V, Kmenta Š, Olejníčk J, Hubička Z and Hippler R 2013 *Thin Solid Films* **549** 177–183
[40] Bobzin K, Brögelmann T, Brugnara R H and Chromy S 2015 *Thin Solid Films* **596** 140–146
[41] Alami J, Sarakinos K, Mark G and Wuttig M 2006 *Appl. Phys. Lett.* **89** 154104
[42] Winter G J, Hecimovic A, de los Arcos T, Böke M and Schulz-von der Gathen V 2013 *J. Phys. D: Appl. Phys.* **46** 084007
[43] de los Arcos T, Layes V, Gonzalvo Y A, Schulz-von der Gathen V, Hecimovic A and Winter J 2013 *J. Phys. D: Appl. Phys.* **46** 335201

[44] Breilmann W, Eitrich A, Maszl C, Hecimovic A, Layes V,Benedikt J and von Keudell A 2015 *J. Phys. D: Appl. Phys.* **48** 295202
[45] Hecimovic A, Böke M and Winter J 2014 *J. Phys. D: Appl. Phys.* **47** 102003
[46] de los Arcos T, Schröder R, Gonzalvo Y A, Schulz-von der Gathen V and Winter J 2014 *Plasma Sources Sci. Technol.* **23** 054008
[47] Kudriavtsev Y, Villegas A, Godines A and Asomoza R 2005 *Appl. Surf. Sci.* **239** 273–278
[48] Vitelaru C, Lundin D, Stancu G D, Brenning N, Bretagne J and Minea T 2012 *Plasma Sources Sci. Technol.* **21** 025010